Supplemental Material

Numerical Simulations. Simulations have been carried out with the finite elements method (FEM) implemented in the commercial COMSOL Multiphysics software. The domain was setup in 3D and truncated by perfectly matched layers to avoid back reflection from the domain walls. Left- and righthand (+ and -, respectively) circularly polarized light at different wavelengths was generated at the top of the simulation domain. The effect of a glass substrate was considered by setting the refractive index to n=1.5 in the bottom half of the simulation domain. For the layer-by-layer simulations, alternating layers of gold and the dielectric were considered. Interpolated refractive index data from Rakic et al. **[1]** for the gold was used. In the numerical simulations, a cylinder is used to model the experimental structures, which rather have a conical shape (see inset of **Fig. 1** in the main text). For this reason, to match the spectral positions of the experimental peaks, the refractive index for the dielectric was kept as free parameter and chosen to be n=2 for TiO_2 and n=1.75 for SiO_2. For the homogenized structures, an effective permittivity was used, calculated according to **Eqs. (1)** and **(2)** in the main manuscript. The current densities j(+H) and j(-H) are numerically obtained from separate simulations, where the direction of the applied magnetic field is inverted along the out-of-plane direction. As proved in the main text, it can be concluded that also the MO response can be described well by using an effective medium description of the permittivity, making these simulations significantly less computationally demanding compared to conventional layer-by-layer approaches.

Analytical modelling. Scattering, absorption and extinction cross sections of isotropic spheres are calculated using a customized Matlab code **[2]** following the formulation of Bohren and Huffman **[3]** for the Mie coefficients a_n and b_n. With the size parameter $x = kr$, where k is the vacuum wave number and r the sphere radius, we can express the scattering and extinction efficiency as

$$Q_{sca} = \frac{2}{x^2}\sum_{n=1}^{\infty}(2n+1)\,(|a_n|^2 + |b_n|^2),$$

$$Q_{ext} = \frac{2}{x^2}\sum_{n=1}^{\infty}(2n+1)\mathrm{Re}(a_n + b_n).$$

Energy conservation requires that $Q_{ext} = Q_{sca} + Q_{abs}$, thus allowing to calculate the absorption efficiency as well. Interpolated refractive index data from Rakic et al. **[1]** for the gold was used also in this case. In our analytical calculations, the system considered is an isotropic sphere. A different value of the dielectric refractive index can then be used to reflect the anisotropy of the system that is otherwise not captured by

isotropic Mie theory. In addition, since we are modelling our system with a sphere, a mismatch between the numerically calculated peaks might appear. For these reasons, to match the spectral positions of the numerically calculated peaks for the TiO_2 case (which is the case we focus on with our analytical calculations), the refractive index of the dielectric was kept as free parameter and chosen to be n=3.5. Importantly, this does not affect the physics of the magneto-optical response, which originates from a change in the metal permittivity induced by the applied magnetic field. This analytical approach is general and can be expanded to other geometries and materials without time constraints related to computational approaches.

Sample fabrication. Hyperbolic metamaterial nanoparticles and control samples (gold nano-disks) were prepared by hole mask colloidal lithography **[4]**. Microscope glass slides were cleaned with acetone and 2-propanol with 2 min sonication, respectively. After deionized water (DI) washing and blow drying under N_2 flow, the glass wafers were ready for the multilayer deposition. For the Au/SiO_2 stacking layer deposition, the glass wafers were loaded into an electron beam deposition (E-beam, PVD75 Kurt J. Lesker company) chamber. One unit of the metal-dielectric bi-layer consisted of 0.5 nm Ti +10 nm Au + 0.5 nm Ti + 20 nm SiO_2, in which Ti served as the adhesion layer. The deposition of the bi-layer unit was repeated five times**.** For the Au/TiO_2 stacking layers, the glass wafers were loaded into an electron beam deposition chamber (Kenosistec KE 500 ET), and 0.5 nm Ti + 10 nm Au + 0.5 nm Ti layers were deposited at a rate of 0.3 Å/s. The wafer was then transferred to an atomic layer deposition chamber (ALD, FlexAL, Oxford Instruments) and TiO_2 was deposited using a process with titanium isopropoxide as the titanium precursor and oxygen plasma as the oxidizer. The process was repeated at 80 °C temperature for 383 cycles to produce a film with a thickness of 20 nm, which was verified with ellipsometry. One unit of the Au/TiO_2 metal dielectric bi-layer consisted of 0.5 nm Ti + 10 nm Au + 0.5 nm Ti + 20 nm TiO_2. The deposition of the bi-layer unit was repeated five times**.** On the top of stacking bilayers, photoresist (950 PMMA A8, Micro Chem) was spin coated at 6000 rpm and soft baked at 100A ℃for 1min. After O_2 plasma treatment (2 min, 100 W, Plasma cleaner, Gambetti), Poly(diallyldimethylammonium chloride) solution (PDDA, Mw 200,000-350,000, 20 wt. % in H2O, Sigma, three times diluted) was drop coated on the top of the PR surface and incubated for 5 min to create a positively charged surface. The extra PDDA solution was washed away under flowing DI water after 5 min incubation. Then negatively charged polystyrene (PS) beads (diameter 552 nm, 5 wt% water suspension, Micro Particle GmbH) were diluted 1: 3 in ethanol and drop casted on the top of the stacking bi-layers; after 30 s the excess was removed under flowing DI water and the sample was dried with N_2 flow. Thereby, randomly distributed PS beads were attached on top of the photoresist. The samples were treated with O_2 plasma etching in the inductively coupled plasma-reactive ion etching system (ICP-RIE, SENTECH SI500) to reduce the size of PS beads. A gold film (40 nm) was

deposited with a sputter system (Sputter coater, Quorum, Q150T ES) on top of the sample to serve as an etching mask to protect the PR underneath. After removal of the PS beads with a Polydimethylsiloxane (PDMS) film, the samples were treated again by O_2 plasma in the ICP-RIE system to etch away the exposed PR which was no longer protected by the PS spheres and create randomly distributed holes as mask on top of the stacking bi-layers. The diameter of the holes was controlled by varying the etching time during the first O_2 plasma treatment performed to reduce the size of the beads. Then, 100 nm of Cr were deposited with the e-beam evaporator at a vertical cathode/target angle of incidence. Followed by liftoff of the PR in acetone, randomly distributed Cr disks on the stacking multilayer were fabricated. With the Cr disk mask, ICP-RIE etching was carried out with CF_4 gas flow 15 sccm, radio frequency (RF) power 200 W, ICP power 400 W, temperature 5 ℃, pressure 1 Pa. The etching time was adjusted according to the stacking film thickness to ensure all the extra stacking bi-layer material, except for the area under Cr mask, was removed. Then the sample was soaked in Cr etchant (Etch 18, OrganoSpezialChemie GmbH) for 2 min to remove the Cr mask. Followed by DI water cleaning and drying under N_2 flow, the sample morphology was characterized with a scanning electron microscope (SEM, FEI Helios NanoLab 650).

Optical and magneto-optical characterization. Extinction spectra have been recorded on a JASCO V-670 commercial spectrophotometer in the 300 - 2700 nm spectral range. MCD spectra were collected using a home-built setup, equipped with a 300 W Xe arc lamp. The output light from a monochromator (Oriel Cornerstone 260) is linearly polarized by a Rochon prism. Circular polarization was then obtained using a photo-elastic modulator (Hinds Instruments PEM-90) able to switch at a rate of 47 kHz between right- and left-circular light polarization. Circularly polarized light is then focused on the sample, which is placed in a water-cooled electromagnet, able to reach 1.4 Tesla at room temperature. A Photomultiplier tube is used as detector for the visible range (300-850 nm), while an InGaAs diode is used for the near infrared spectral range (750-2200 nm). Light propagation was set parallel to the applied magnetic field. The dichroism signal was recorded by lock-in detection at the modulation frequency. The static signal is further modulated at 440 Hz using a mechanical chopper to filter out the residual environmental light, and subsequently analyzed by a second demodulation. The MCD signal is obtained as the ratio between the signal modulated by the PEM and the one modulated by the chopper. To avoid offset issues and spurious natural dichroism coming from the setup, the final MCD spectrum is obtained by subtraction of two spectra recorded at the same magnetic field but with opposite sign. The magnitude of the dichroism signal (ΔA) was calibrated through a standard technique using a $Fe(CN)_6^{3+}$ solution as a reference **[5]**.

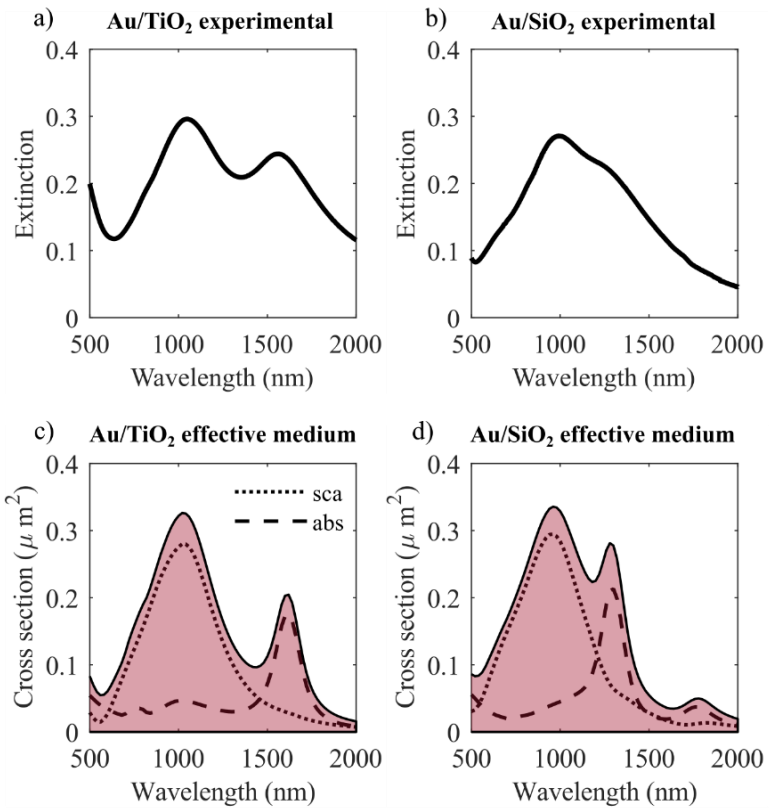

SUPPLEMENTAL FIG. 1. Experimental extinction (a and b) and simulated scattering (dotted lines) and absorption (dashed lines) cross sections (c and d) for the Au/TiO_2 and the Au/SiO_2 samples as a function of the wavelength of the incoming light.

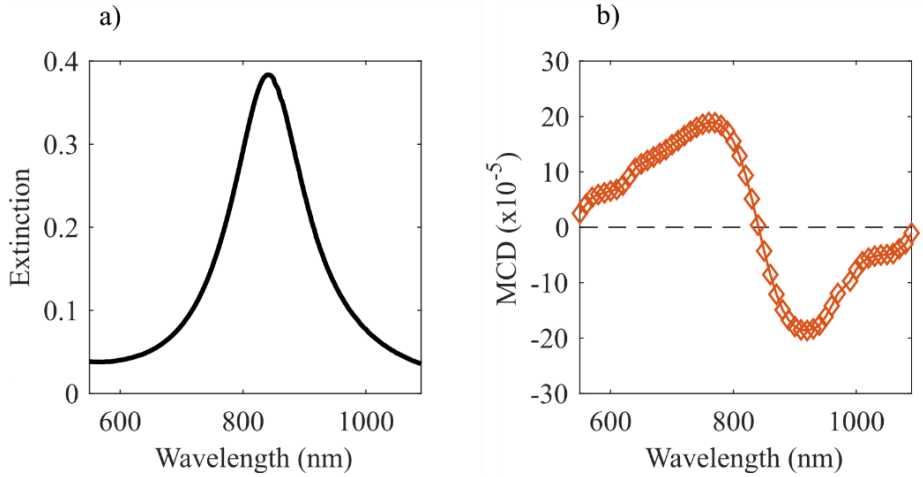

SUPPLEMENTAL FIG. 2. Experimental extinction (a) and MCD (b) spectra of plain Au nanodisks.

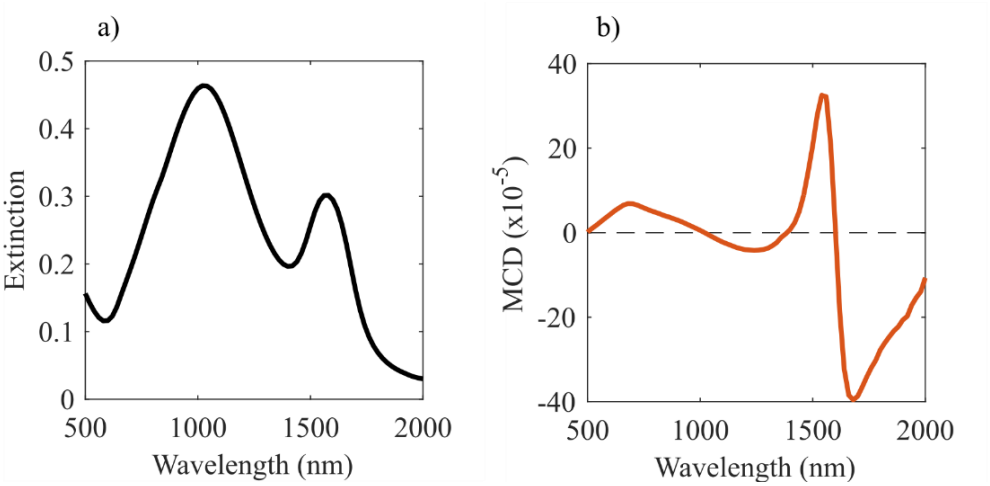

SUPPLEMENTAL FIG. 3. Numerical extinction (a) and MCD (b) spectra of the hybrid Au/TiO_2 structure using a frequency dependent off-diagonal permittivity $\varepsilon_{MO}(\omega) = i\varepsilon(\omega)\frac{\omega_c}{\omega+i\gamma}$, where $\varepsilon(\omega)$ is the diagonal permittivity, ω_c is the cyclotron frequency and γ is the electronic relaxation constant.

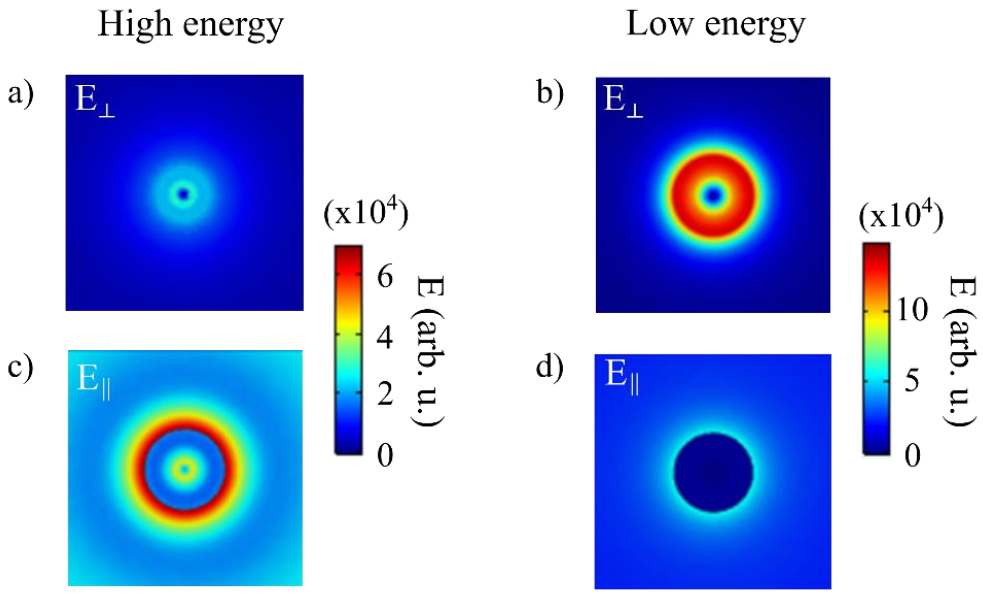

SUPPLEMENTAL FIG. 4. Electric near-field plots of a single hyperbolic Au/TiO2 nanodisk at the high (a and c) and low (b and d) energy resonance for the in- and out-of-plane component of the field, respectively. X-Y cuts are taken in the middle of the structure. While the in-plane component dominates at the high energy resonance, the out-of-plane component majorly contributes at the low energy resonance.

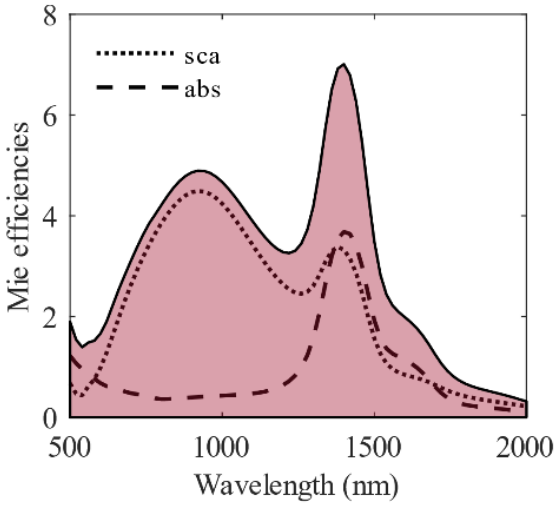

SUPPLEMENTAL FIG. 5. Numerically calculated scattering (dotted line) and absorption (dashed line) efficiencies of a sphere with r =150 nm considering anisotropic permittivity $\hat{\varepsilon} = (\varepsilon_{\parallel}, 0,0; 0, \varepsilon_{\parallel}, 0; 0,0, \varepsilon_{\perp})$. While scattering dominates at the high energy resonance, we find an equal contribution of scattering and absorption at the low energy resonance.

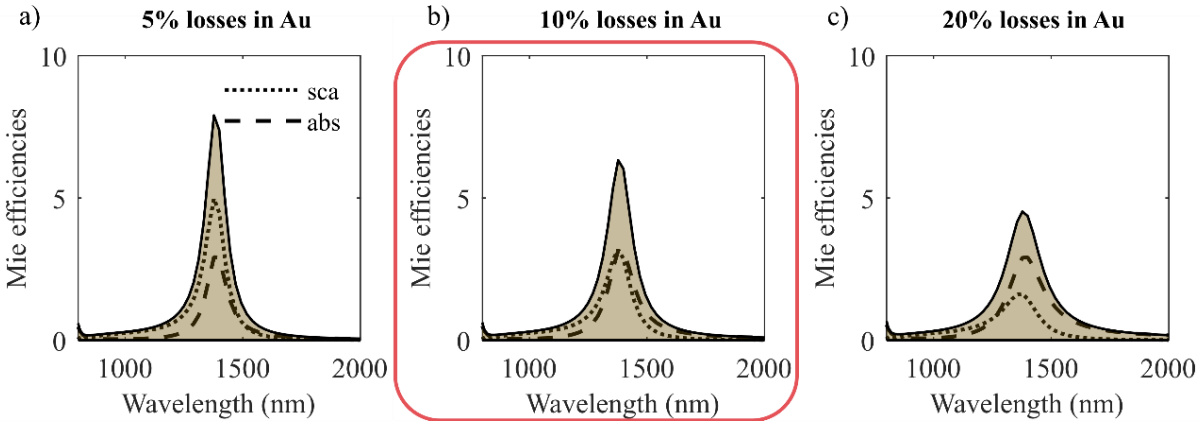

SUPPLEMENTAL FIG. 6. Calculated scattering (dotted lines) and absorption (dashed lines) efficiencies of the out-of-plane magnetic dipole term in the Mie expansion of the optical extinction. A small fraction (5% (a), 10% (b) and 20% (c)) of the imaginary part of the metal permittivity is added to the out-of-plane dielectric function to account for non-radiative losses in gold. A fraction of 10 % (marked by the red box) yields equal contribution of scattering and absorption, representing well the numerical results for real anisotropic particles at the low energy resonance shown in Supplemental Fig. 5.

[1] A. Rakić, A. Djurišić, J. Elazar, and M. Majewski, "Optical properties of metallic films for vertical-cavity optoelectronic devices," Appl. Opt. **37**, 5271

[2] C. Matzler, "MATLAB functions for Mie scattering and absorption," IAP Res. Rep. No. 2002-11 (2002).

[3] C. F. Bohren and D. R. Huffman, "Absorption and scattering of light by small particles," John Wiley & Sons (2008).

[4] H. Fredriksson, Y. Alaverdyan, A. Dmitriev, C. Langhammer, D. S. Sutherland, M. Zäch, and B. Kasemo, "Hole–mask colloidal lithography," Adv. Mater. **19**, 4297 (2007).
[5] W. R. A. Mason, "A practical guide to magnetic circular dichroism spectroscopy," Wiley-Interscience (2007).